Title

Microneedle-Based Continuous Levodopa Monitoring in Patients with Parkinson's Disease

Journal

ACS Sensors

ISSN

2379-3694

Authors

Reynoso, Maria

Moonla, Chochanon

Longardner, Katherine

et al.

Publication Date

2026-07-28

DOI

10.1021/acssensors.6c02083

ACS SENSORS

pubs.acs.org/acssensors Article

Microneedle-Based Continuous Levodopa Monitoring in Patients with Parkinson's Disease

Maria Reynoso,[+] Chochanon Moonla,[+] Katherine Longardner,[+] Nuenghathai Chaiya, Stacey Surace, An-Yi Chang, Tamoghna Saha, Umair Mahmood, Muhammad Khan, Michael Skipworth, Ian McGregor, Ava Van Damme, Lidia F. Vazquez, Eshita Shah, Hao Luan, Irene Litvan,* and Joseph Wang*

Cite This: https://doi.org/10.1021/acssensors.6c02083 Read Online

ACCESS | Metrics & More | Article Recommendations | Supporting Information

ABSTRACT: Optimal levodopa (L-Dopa) dosing for the personal management of Parkinson's disease represents a major clinical challenge due to L-Dopa's narrow therapeutic window and inter- and intra-patient absorption variability. Current methods for measuring L-Dopa, relying on repeated blood draws for centralized laboratory measurements, fall short of capturing dynamic L-Dopa fluctuations that are relevant for timely interventions. Here, we present a minimally invasive microneedle (MN)-based wearable biosensor for continuous monitoring of L-Dopa (CDM) in human subjects. The MN biosensor platform relies on a tyrosinase-functionalized working electrode for detecting L-Dopa in interstitial fluid (ISF) through enzymatic electrochemical detection. The device was evaluated in healthy volunteers and participants with Parkinson's disease in clinical settings, illustrating its ability to provide actionable temporal insights. Critical validation of the MN biosensor was carried out by comparing the ISF L-Dopa signals with plasma L-Dopa concentrations measured by high-performance liquid chromatography (HPLC). Using subject-specific calibration and lag-time correction, the ISF-derived drug profiles showed a close correlation with plasma L-Dopa pharmacokinetics, with a mean absolute relative difference (MARD) of 9.64%. An inverse correlation between the L-Dopa pharmacokinetics and the corresponding motor performance was observed. Such pioneering demonstration of the clinical feasibility of MN-based CDM in humans highlights its considerable potential for supporting the management of Parkinson's disease.

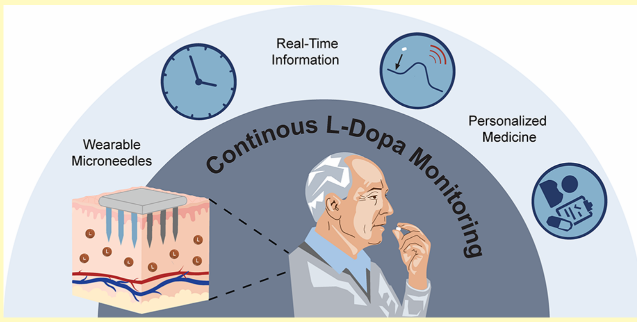

KEYWORDS: *microneedles, continuous monitoring, wearable biosensor, Parkinson's disease, enzymatic electrochemical detection, levodopa*

Parkinson's disease (PD) is a progressive neurodegenerative condition that impairs motor function. It results from the gradual deterioration of dopamine-producing neurons in the substantia nigra. The loss of the neurotransmitter dopamine leads to progressive motor symptoms, which include tremors, bradykinesia (slowed movement), rigidity (muscular stiffness), and postural instability, along with cognitive impairment, sleep disturbances, and mood disorders.[1] PD is the second most common neurodegenerative disorder, affecting nearly 10 million people worldwide.[2,3] With increasing life expectancy, PD cases are projected to double by 2040, imposing an enormous global economic burden and highlighting the urgent need for more effective therapeutic interventions.[4−6] Despite significant research efforts, no cure for PD currently exists, so treatment focuses on alleviating symptoms, primarily through dopamine replacement therapies.[7−9]

One major challenge of treating PD symptoms is that dopamine cannot be administered directly because it cannot cross the blood-brain barrier (BBB). Alternatively, levodopa (L-Dopa) - a precursor to dopamine - can cross the BBB, where it is converted to dopamine by the enzyme dopa decarboxylase.[10−12] L-Dopa is usually co-administered orally with a dopa decarboxylase inhibitor (e.g., carbidopa), which prevents peripheral conversion of L-Dopa before it reaches the brain, enabling a greater concentration to reach the central nervous system and reducing side effects such as nausea and low blood pressure.[13,14] Although L-Dopa remains the most effective pharmacological treatment for PD motor symptoms, there are several limitations to its use. Frequent L-Dopa doses must be taken (at minimum 2−3 times daily) due to its short half-life. Furthermore, several gastrointestinal factors may impair L-Dopa's absorption, including food intake, concurrent medications, and constipation.[15] Over time, with increasing dopaminergic deficiency, L-Dopa's therapeutic window narrows, often requiring more frequent and higher doses to maintain its

Received: May 13, 2026
Revised: July 2, 2026
Accepted: July 7, 2026

beneficial effects. People with advanced PD may experience fluctuating symptoms, with varying and often unpredictable responses to L-Dopa doses and reemergence of parkinsonian symptoms ("off" time) when L-Dopa levels are subtherapeutic, and dyskinesias (excessive involuntary movements) when L-Dopa levels are therapeutic or supratherapeutic.[12] While L-Dopa is considered the "gold standard" for treating PD motor symptoms,[16] routine clinical practice lacks reliable tools for real-time L-Dopa monitoring, making timely personalized dosing strategies difficult to achieve. Addressing this gap is critical for maintaining optimal therapeutic drug levels, improving clinical outcomes, and reducing the overall burden of PD.[17,18]

Current methods for L-Dopa monitoring are time-consuming and require invasive blood extraction, complex sample preparation, trained lab technicians, and specialized, bulky, centralized instrumentation, ranging from high-performance liquid chromatography (HPLC) to liquid chromatography-mass spectrometry (LC-MS), making such L-Dopa assays unsuitable for real-time monitoring or point-of-care (POC) applications.[12,19−21] These limitations underscore the need for alternative, minimally invasive, and rapid L-Dopa decentralized or wearable detection methods. Disposable L-Dopa electrochemical sensor strips have been developed for frequent POC testing of the drug in blood and sweat biofluids.[22,23] However, such disposable sensors cannot capture L-Dopa dynamics and support optimal L-Dopa dosing.

In this study, we introduce and demonstrate for the first time a wearable microneedle (MN)-based sensing platform for continuous L-Dopa monitoring (CDM) in both healthy volunteers and participants with PD (Figure 1a). Wearable electrochemical MN sensors have gained a tremendous recent interest towards the reliable minimal-invasive monitoring of biomarkers in interstitial fluid (ISF).[24,25] An initial proof-of-concept electrochemical MN sensing platform for L-Dopa measurements was demonstrated in-vitro using skin-mimicking phantom gels and mice skin penetration.[5] More recently, a stainless-steel microneedle array patch was tested for L-Dopa monitoring in living rats.[10] Critically, no L-Dopa MN sensing devices have progressed to human clinical trials, leaving a major translational gap. Key challenges remain in terms of assessing the on-body performance of L-Dopa MN sensors in persons with PD, patient comfort, safety, and tolerability, operational stability over extended wear, long-term biocompatibility and correlation with motor symptoms. Addressing these limitations and gaps is essential for realizing highly reliable and stable MN L-Dopa monitoring platforms and eventually towards enabling closed-loop PD drug management systems that could minimize motor fluctuations, improve quality of life, and reduce the healthcare burden associated with PD.

The new MN wearable device is based on a two-electrode electrochemical system consisting of a tyrosinase (TYR)-modified working electrode and a platinum reference electrode, enabling enzymatic conversion of L-Dopa to dopaquinone, which is detected cathodically at a negative potential (Figure 1a). The MN L-Dopa monitoring platform offers an attractive minimally invasive, patient-friendly system for capturing real-time pharmacokinetic and pharmacodynamic profiles (Figure 1e−i). CDM was performed in PD patients alongside motor symptom score assessments and blood pressure monitoring. The L-Dopa measurements from human subjects were validated against plasma L-Dopa concentrations measured by the current "gold standard" high-performance liquid chromatography (HPLC). Both ISF and plasma L-Dopa levels showed an inverse correlation with motor scores, where higher motor scores (indicating worse symptoms) were associated with lower L-Dopa concentrations. This relationship is consistent with the pharmacodynamic role of L-Dopa in symptom control and supports the utility of continuous monitoring for real-time therapeutic assessment.

These initial human clinical trials highlight the potential of CDM to capture dynamic L-Dopa fluctuations that are inaccessible through common intermittent blood sampling. The MN-based CDM device accurately reflects the L-Dopa pharmacokinetic changes following oral L-Dopa administration in patients with PD. Such capability is particularly relevant for managing motor complications, including wearing-off phenomena and dyskinesias, which are closely linked to fluctuations in L-Dopa levels[26−30] (Figure 1d). Subject-specific lag times between L-Dopa concentrations in ISF and blood were identified, and individualized calibration was applied to account for these delays (Figure 1b,c). Correlation analyses using Pearson statistics, Bland-Altman plots, and mean absolute relative difference (MARD) confirmed the reliable performance of the MN L-Dopa biosensor (MARD of 9.64% in participants with PD). By enabling continuous individualized tracking of L-Dopa, this approach provides actionable temporal insights and supports data-driven, timely, optimized dosing in PD, paralleling the transformative impact of continuous glucose monitoring (CGM) in diabetes care, and addressing a critical translational gap in the management of PD.

METHODS

Materials

All reagents and solvents were used as received without further purification. Acetaminophen ($C_8H_9O_2N$, ≥98.0%), L-ascorbic acid ($C_6H_8O_6$, 99%), bovine serum albumin from lyophilized powder (BSA, pH 7, ≥98%), carbidopa ($C_{10}H_{14}N_2O_4{\cdot}H_2O$, C-Dopa)3,4-dihydroxy-l-phenylalanine (L-Dopa), dopamine hydrochloride (≥98%), D-(+)-glucose anhydrous ($C_6H_{12}O_6$, ≥99.5%), glutaraldehyde solution ($C_5H_8O_2$, 50 wt % in H_2O), L-(+)-lactic acid ($C_3H_6O_3$, ≥98%), Nafion (5 wt % in a mixture of lower aliphatic alcohols and water), phosphate buffer solution (1.0 M, pH 7.4), poly(vinylchloride), sodium lactate ($C_3H_5NaO_3$, USP), tyrosinase (from mushroom, EC 1.14.18.1, lyophilized powder, ≥1000 unit mg^{-1} solid), L-tyrosine hydrochloride (98%), and uric acid ($C_5H_4N_4O_3$, ≥99%) were purchased from Sigma-Aldrich. Artificial ISF was prepared according to our earlier report.[31] Fava beans were obtained from a local store.

Microneedles Fabrication and Device Assembly

All parts (MN, cover, and bracket) were designed and adapted using SolidWorks software (Figure 1e). *Microneedles:* The microneedle array has a total of 20 microneedles, with 10 serving as the working electrode (WE) while the other 10 as the reference electrode (RE). These arrays were fabricated via 3D printed using Digital Light Processing (DLP) printing (Kudo3D model: micro15) (Supporting Information Figure 1a(i)), as we reported earlier.[32,33] After printing, the parts were cleaned in an isopropanol ultrasonic bath for 60 min and then were UV-cured (405 nm, Kudo3D) for 30 min. Subsequently, the microneedles were outgassed at 80 °C overnight. Subsequently, the microneedles were masked and prepared for the metal deposition step, where a layer of chromium, followed by a platinum layer, were sputtered onto the microneedle (with a Cr adhesion layer for 6 min at 300 W and a Pt layer for 15 min at 100 W) using 65% rotation and 2.41 mTorr Ar gas pressure in a Denton Discovery 635 machine (Figure 1g and Supporting Information Figure 1a(ii,iii),b(ii)). *Cover and Bracket:* These parts were fabricated via stereolithography (SLA) 3D printing using a Form3 printer

https://doi.org/10.1021/acssensors.6c02083
ACS Sens. XXXX, XXX, XXX−XXX

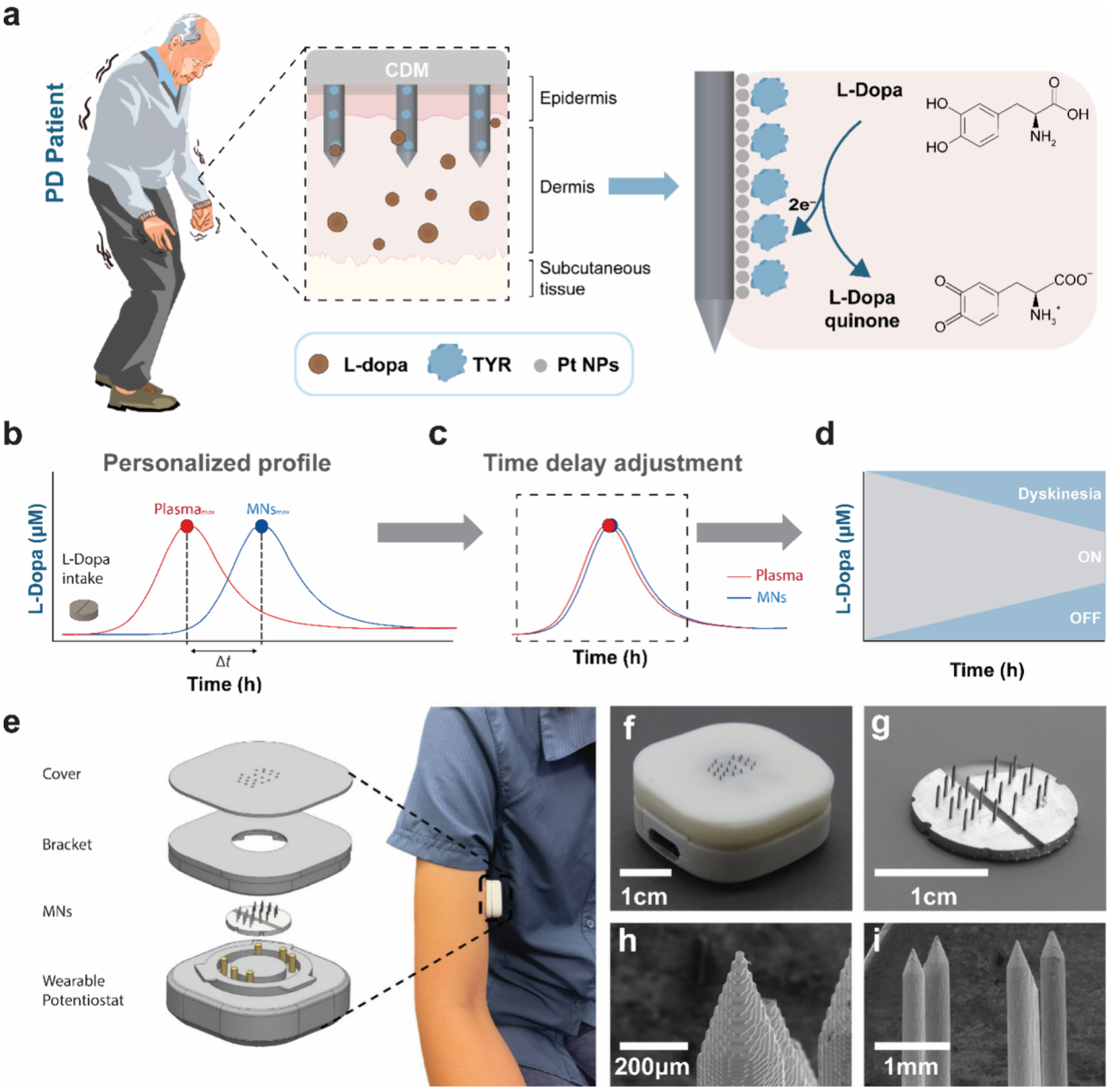

Figure 1. Concept of real-time continuous monitoring of L-Dopa in interstitial fluid (ISF) in participants with Parkinson's disease (PD). (a) The wearable microneedle (MN) patch is applied on the skin of the person with PD for continuous L-Dopa monitoring of L-Dopa in ISF. The MN surface is functionalized with the enzyme tyrosinase (TYR) to catalyze the oxidation reaction of L-Dopaquinone for electrochemical detection. (b) Personal identification of the lag-time between ISF and plasma L-Dopa were established, proceeding to (c) time delay adjustment for concentration translation. (d) These types of profiles can inform in real time L-Dopa dose adjustments and improve symptom management. (e) Exploded schematic representation of the wearable MN device, which consists of a top cover for electrode isolation, and the mounting bracket for adaptability to the commercial wearable potentiostat for signal acquisition and transmission via Bluetooth. The fully assembled device is shown on the upper arm. (f) Photograph of the wearable MN sensing device. (g) Photographs of the MN array after metal deposition. (h, i) SEM images of the MNs after sputtering.

(White resin, Formlabs). After printing, the parts were cleaned in an isopropanol ultrasonic bath for 30 min and then UV-cured (405 nm, FormCure) for 15 min (Supporting Information Figure 1b(i,iv)). *Device assembly:* First, the microneedle array was attached to the bracket. The base of the microneedles has 6 semi-holes on the outer diameter that served as guides to fit to the bogo pins of the wearable potentiostat (Sensit Wearable, PalmSens). Second, we added a thin layer of photocurable resin at the base of the microneedles and bracket to attach the cover piece. This piece facilitated electrical insulation and the desired microneedle height. The resin was cured using a UV-lamp (SUNUV 365 nm UV and 405 nm LED light) for 200 s on the double power setting. Lastly, the bracket integrated with the microneedles was mounted onto the wearable potentiostat (Supporting Information Figure 1b(i,iii)). This fabrication resulted in microneedles with approximately 25 μm in tip size, 300 μm in diameter and 700 μm in height, as illustrated in the SEM image of Supporting Information Figure 2. SEM images were taken using a FEI Quanta 250 SEM.

Development of the L-Dopa Microneedle Sensor

The modification of the microneedle working electrode relied on a drop cast technique. The enzyme solution, tyrosine oxidase (4 mg ml^{-1}), was prepared in BSA (10 mg ml^{-1} in 0.1 M PBS). Four layers (5 μl) of enzyme solution were drop casted on top of the microneedles, followed

https://doi.org/10.1021/acssensors.6c02083
ACS Sens. XXXX, XXX, XXX−XXX

by the addition of 2 v/v % glutaraldehyde in distilled water (5 μl), followed by casting 5 μl of a 2% Nafion solution (in DI water). Finally, on all working microneedles, a protective layer consisting in a solution of 2 wt % polyvinyl chloride (in tetrahydrofuran with 1 mM Triton X-100) was cast to avoid leaching and biofouling problems (Figure 2a). After modification, the patches were stored overnight in the fridge (4 °C) for further in vitro and on-body testing (Figure 3).

Skin Insertion Evaluation

Following the modification of the MNs, the sensing interface was examined before and after skin insertion to evaluate potential detachment or damage of the reagent's coatings. As shown in the SEM images (Supporting Information Figure 2), the MNs exhibited no evident delamination or geometry deformation after skin insertion, indicating that both the coating and the overall microneedle geometry were well preserved after insertion.

In Vitro Evaluation

The sensing performance of the developed L-Dopa microneedle sensors were evaluated by amperometric measurements in 0.1 M PBS (pH 7.4) spiked with standard L-Dopa solutions, using an applied potential of −0.3 V vs Pt for 60 s. A handheld wireless potentiostat (Sensit BT, PalmSens), operated via PSTrace software (version 5.10) was employed for data acquisition, and the results were plotted using Origin software. L-Dopa stock solutions were prepared in 0.1 M PBS (pH 7.4) for all experiments (Figure 2 and Supporting Information Figure 3)

In Vitro Cytotoxicity Assessment

To evaluate cytocompatibility, the microneedles were incubated with THP-1 cells cultured in RPMI-1640 medium (Thermo Fisher Scientific, Waltham, MA) at a concentration of 1×10^6 cells/mL. Prior to exposure, all microneedles were sterilized using UVC irradiation for 1 h. As the present pilot study was designed to evaluate the short-term continuous L-Dopa monitoring, with device wear durations of less than 4 h in both healthy participants and patients with PD, a 24 h in vitro cytotoxicity assessment was performed to evaluate the biocompatibility of the device within the intended operating timeframe. The samples were co-incubated with the cell suspension for 24 h at 37 °C under standard cell culture conditions. Following incubation, 50 μL of

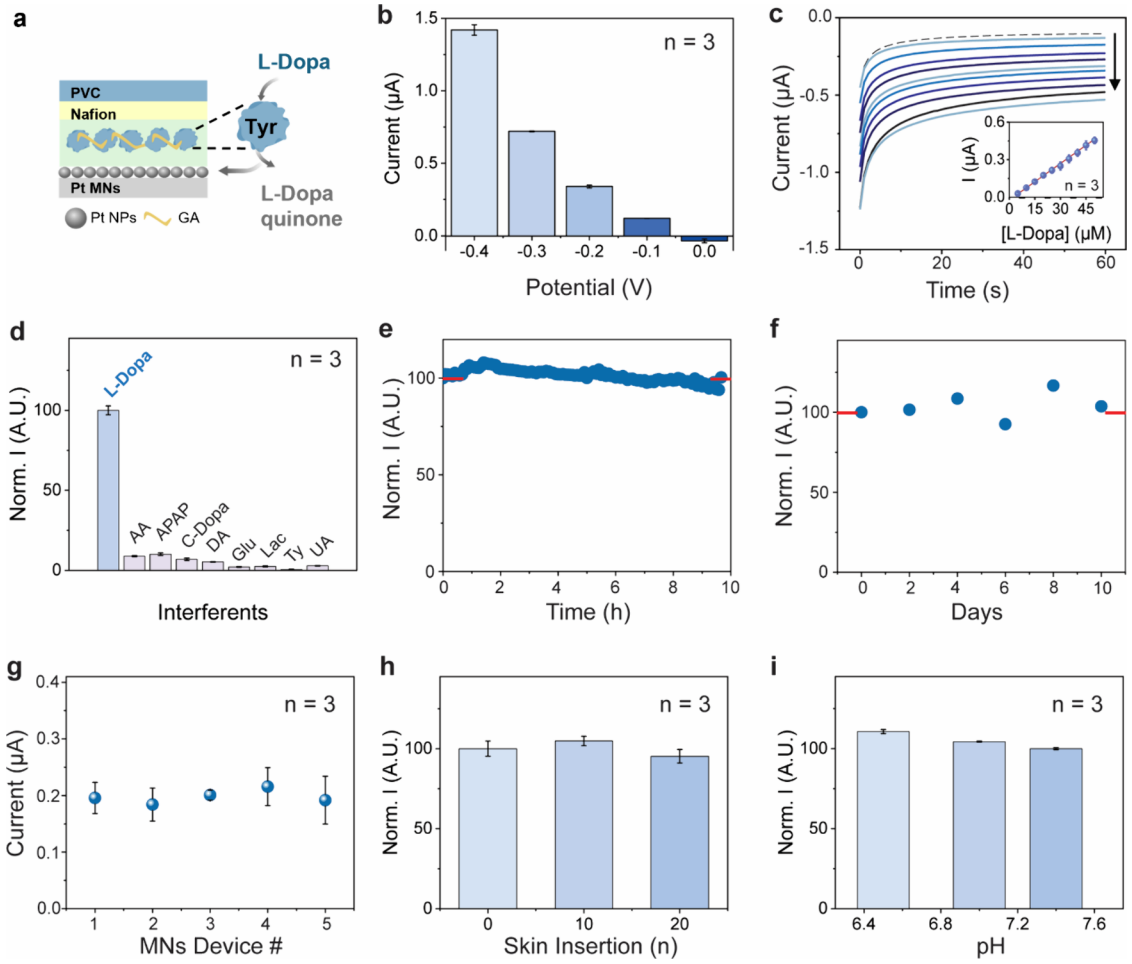

Figure 2. In vitro evaluation of the L-Dopa MN sensor. (a) Schematic of the reagent configuration on the MN working electrode, with a Pt-sputtered surface modified with tyrosinase (Tyr) in BSA, followed by Nafion and PVC layers. Alongside the enzymatic reaction and electrochemical detection mechanism of the dopaquinone product. (b) Effect of applied potentials (0 to 0.4 V vs Pt MNs) on the response of the L-Dopa MN sensor to 1 mM L-Dopa in artificial ISF. (c) Chronoamperograms of the L-Dopa MN sensor upon successive 5 μM L-Dopa additions (up to 50 μM) at −0.3 V vs Pt MNs (Inset: calibration plot). (d) Selectivity study: corresponding current percentage responses to 10 μM L-Dopa vs potential interferents, including 10 μM ascorbic acid (AA), 100 μM acetaminophen (APAP), 2.5 μM carbidopa (C-Dopa), 1 μM dopamine (DA), 1 mM glucose (Glu), 1 mM lactic acid, 10 μM tyrosine (Ty), and 100 μM uric acid (UA). (e) Stability: chronoamperometric responses to 10 μM L-Dopa at 5-min intervals over 580 min (~9.67 h). (f) Shelf life: responses to 10 μM L-Dopa over 10 days. (g) Reproducibility: responses to 10 μM L-Dopa across five MNs devices ($n = 5$). (h) Skin insertion and (i) pH effects on responses to 10 μM L-Dopa.

https://doi.org/10.1021/acssensors.6c02083
ACS Sens. XXXX, XXX, XXX−XXX

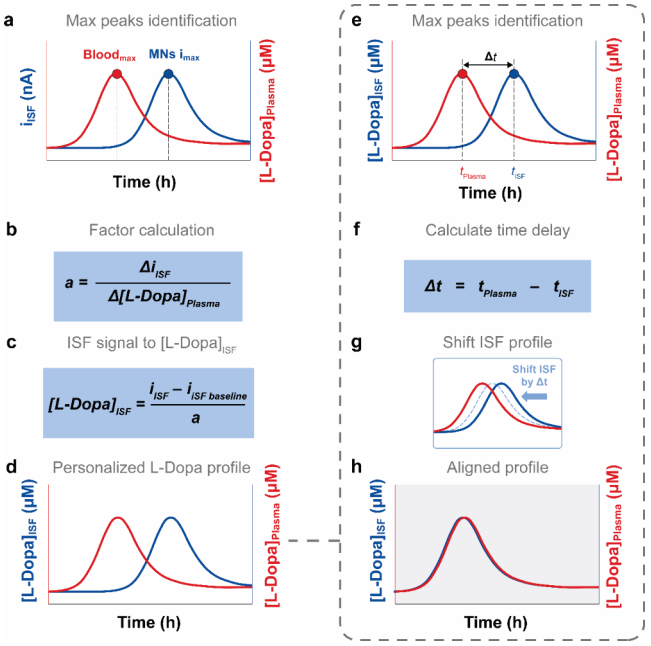

Figure 3. Data processing workflow for converting the MN current signals to ISF L-Dopa concentrations and adjusting for temporal alignment: (a) Identification of the maximum concentration peak in plasma and the corresponding maximum current response in ISF, (b) Calculation of the slope by dividing the change in ISF current (Δi) by the change in plasma L-Dopa concentration (Δ[L-Dopa]), (c) Computation of the ISF L-Dopa concentration by subtracting the baseline ISF current and dividing by the slope. (d) Generation of the converted ISF L-Dopa concentration profile. Temporal alignment of MN response to account for delay: (e) Identification of peak times in plasma and ISF profiles, (f) Determination of the time difference between peaks, (g) temporal shifting of the ISF profile based on the delay, and (h) Plotting of the aligned profiles to define the overlap window for subsequent statistical analysis.

3-(4,5-dimethylthiazol-2-yl)−5-(3-carboxymethoxyphenyl)−2-(4-sulfophenyl)-2H-tetrazolium (MTS) reagent (colorimetric assay, ab197010) was added to 500 μL of each well's cell suspension and the mixture was further incubated for 30 min at 37 °C. Such MTS assay was selected because, while it is based on the same tetrazolium reduction mechanism as the traditional MTT assay (3-(4,5-dimethylthiazol-2-yl)−2,5-diphenyl-2H-tetrazolium bromide), it produces a water-soluble formazan product that eliminates the need for an additional crystal-dissolution step, thereby simplifying the assay protocol while reducing the experimental variability. The absorbance at 490 nm was measured using a BioTek Synergy Mx microplate reader to determine cell viability (Supporting Information Figure 4).

Battery Life Optimization

The Sensit wearable software was initially set to continuous monitoring mode, where the device continuously recorded signal data and transmitted it via Bluetooth. This resulted in rapid battery consumption, limiting the battery life to approximately one hour. In this study, we rewrote the device's code to optimize power consumption by applying sleep mode during the 5-minute waiting period. During this interval, the Sensit wearable device stops recording signals and disables Bluetooth transmission to conserve energy. After 5 min, the device automatically wakes up and restarts data recording for 30 s. To monitor baseline fluctuations, the updated code records a new baseline before each 5-minute measurement interval. Moreover, since the device includes two operational channels, the updated code enables only one, keeping the second channel disabled to minimize energy usage. This reduced power consumption significantly extends the device's battery life up to 6 h.

Eligibility Criteria for L-Dopa Monitoring

Healthy Participants for Fava Bean Consumption. Eligible healthy participants had no active medical problems and were at least 18 years old, able to provide informed consent, and willing to consume fava beans during the study and abstain from caffeine on the day of the study. Exclusion criteria were current pregnancy or active nursing, allergy or intolerance to fava beans; and inability to comply with study dietary restrictions.

Healthy Participants for Ingestion of the Oral Carbidopa/L-Dopa Immediate-Release Tablet. Eligible participants were at least 18 years of age, had no active medical problems (e.g., diabetes mellitus, heart failure, cardiac arrhythmia, or cancer), were able to provide informed consent, and were willing to abstain from caffeine and high-protein foods on the day of the study visit. Exclusion criteria were current pregnancy or actively nursing; hypotension, use of non-selective monoamine oxidase inhibitors within the previous two weeks; a history of glaucoma, psychosis, peptic ulcer disease, malignant melanoma, myocardial infarction, or cardiac arrhythmias; and any other condition that, in the opinion of the investigators, would place the participant at increased risk.

PD Patients for Ingestion of the Oral Carbidopa/L-Dopa Immediate-Release Tablet. All potential participants met the Movement Disorder Society (MDS) diagnostic criteria for clinically established PD, which are highly sensitive and specific.[34,35] General inclusion criteria included age between 40 and 85 years, the ability to provide signed informed consent in English or Spanish, and a diagnosis of mild, moderate, or severe PD corresponding to Hoehn and Yahr stages I−IV (able to walk).[36] Participants were required to be receiving immediate-release oral carbidopa/L-Dopa therapy and either not taking or taking stable doses of other antiparkinsonian medications, including dopamine agonists, monoamine oxidase B (MAO-B) inhibitors, or catechol-O-methyltransferase (COMT) inhibitors. General exclusion criteria were other neurological conditions, including, but not limited to stroke, dementia, including PD dementia,[37] and traumatic brain injury; uncontrolled active medical conditions such as heart or liver failure or uncontrolled diabetes; prior deep brain stimulation device placement; use of nonselective monoamine oxidase inhibitors within the previous two weeks; hypotension; a history of glaucoma, peptic ulcer disease, malignant melanoma, myocardial infarction, cardiac arrhythmias, or psychosis; current pregnancy or breastfeeding; and any other condition that, in the opinion of the investigators, would place the participant at increased risk.

Microneedle Sensor Testing in Healthy Subjects after Fava Bean Consumption

Healthy volunteers used the MN device for approximately 2−3 h under an approved University of California San Diego (UCSD) IRB protocol (Project #171927). The MN sensor was placed on each participant using 3M double-sided medical tape. Current signals were recorded by chronoamperometry under optimized experimental conditions. After one hour of baseline stabilization, subjects consumed 450 g of fully cooked fava beans within a five-minute period. For validation, finger-pricked capillary blood samples were collected every 10 min and analyzed for L-Dopa concentration using biosensor strips previously reported by our laboratory[22] (Supporting Information Figure 5).

Testing in Healthy Subjects after Ingestion of an Oral Carbidopa/L-Dopa Immediate-Release Tablet

All study visits were conducted in a private room at the UCSD Altman Clinical and Translational Research Institute (ACTRI) clinic space under an IRB-approved protocol (Project # 201535). All participants provided written informed consent. Participants' eligibility for the study was confirmed through a review of medical history and a physical examination by a neurologist. The MN sensor was placed on each participant using 3M double side medical tape for approximately 3 h, and

https://doi.org/10.1021/acssensors.6c02083
ACS Sens. XXXX, XXX, XXX−XXX

current signals were recorded by chronoamperometry under optimized experimental conditions. After baseline stabilization for approximately 90 min, each subject received one immediate-release oral tablet containing A3B2 25 mg carbidopa/100 mg L-Dopa. For sensor validation, blood draws samples were collected every 10 min by a nurse, processed after collection, and sent to the HPLC Bioanalytical Core, Emory University School of Medicine for plasma L-Dopa concentration analysis via HPLC. To ensure participant safety, nursing staff measured vital signs, including heart rate and blood pressure every 10 min (Figure 4 and Supporting Information Figure 6).

Testing in Participants with PD after Ingestion of Oral Carbidopa/L-Dopa Immediate-Release Tablets

All study visits were conducted in a private room at the UCSD ACTRI clinic space under the same IRB-approved protocol (Project #201535). All participants provided written informed consent. Participants' eligibility for the study was confirmed through review of their medical histories and physical examination by a movement disorders neurologist. All participants with PD attended two visits: one screening visit and one study visit. If participants met all eligibility criteria at the screening visit, they returned for a study visit, before which they held antiparkinsonian medication for at least 10 h. On the morning of the study, they were also asked to abstain from consuming caffeine, which may interfere with HPLC analysis,[38] and from foods containing high amounts of protein (e.g., protein shakes, animal products), which may alter L-Dopa's bioavailability.[39] On the day of the study, the MN sensor was placed on each participant using 3M double-sided medical tape and worn for approximately three hours in total. Current signals were recorded via chronoamperometry at −0.3 V. After baseline stabilization for approximately 70 min, each subject ingested oral immediate-release carbidopa/L-Dopa, with the dose determined by each participant's their home regimen. More detailed information about the participants can be found in Supporting Information Table 1.

For sensor validation, an intravenous catheter was placed in an antecubital vein. Blood samples were drawn every 10 min by a nurse for approximately 2 h, processed after collection, and sent to the HPLC Bioanalytical Core, Emory University School of Medicine for L-Dopa concentration analysis via HPLC. In parallel, motor performance was evaluated every 10 min based on a modified Movement Disorder Society-Unified Parkinson's Disease Rating Scale (MDS-UPDRS) Part III.[36,40] The standardized evaluation included ratings of rest tremor, action tremor (postural and kinetic), rigidity, and bradykinesia/hypokinesia (finger taps, hand grips, pronation/supination, toe taps, and heel stomps), with each item scored on an ordinal 0−4 scale (0 = normal, 4 = severe impairment) (Supporting Information Figure 7). The total score was recorded for each time point to capture changes in motor performance following L-Dopa administration. To verify that patient movement (tremor or dyskinesia) did not influence the sensor performance, additional control tests were conducted, confirming that motion had a negligible effect on the current response or the overall sensing performance (Supporting Information Figure 8). Lastly, to ensure safety, nursing staff measured heart rate and blood pressure every 10 min (Figure 5 and Supporting Information Figure 9).

Plasma Sample Handling Process after Collection, Storage Conditions, and Shipping

The EDTA Vacutainers (lavender top) were placed on wet ice 15 min before the blood draws by the study coordinator. Immediately after

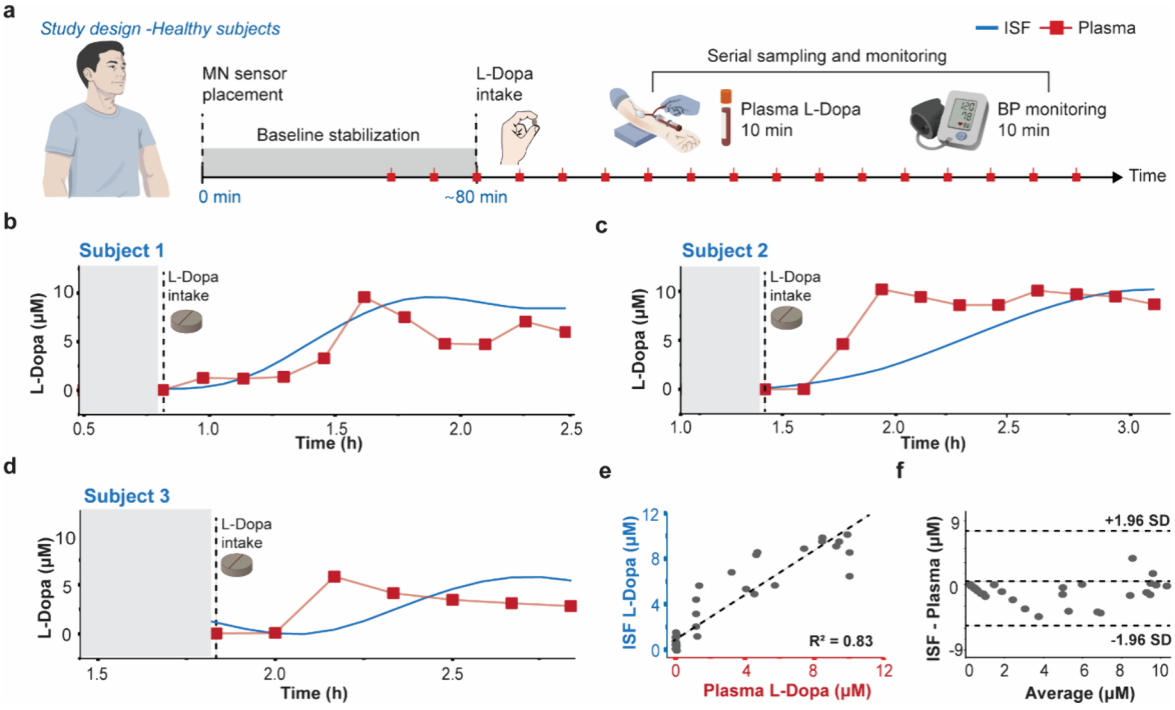

Figure 4. On-body monitoring of L-Dopa dynamics using a wearable MN device in healthy human subjects. (a) Experiment workflow followed to evaluate the wearable microneedle sensor in healthy participants. L-Dopa$_{ISF}$ monitoring begins with a stabilization period to ensure a steady baseline signal. In parallel, L-Dopa$_{Plasma}$ monitoring is performed through venous blood draws collected every 10 min. After baseline stabilization, subjects took one oral tablet of immediate-release 25 mg carbidopa/100 mg L-Dopa. Throughout the study, blood pressure (BP) was measured every 10 min. (b−d) Real time profiles of L-Dopa concentrations measured in ISF using the MN device (blue) and in plasma using HPLC (red) from three healthy volunteers. Oral administration of the carbidopa/L-Dopa tablet was performed following the stabilization period, indicated by the grey-shaded region. (e) Correlation between ISF L-Dopa concentrations obtained via the MN device and the corresponding L-Dopa plasma concentrations measured by HPLC across all subjects. A strong linear relationship ($R^2 = 0.83$) was observed, calculated while applying delay-time correction. (f) Bland−Altman analysis comparing L-Dopa concentrations measured in ISF and plasma. The plot shows the mean difference (dashed line) and the ±1.96 SD limits of agreement (solid red lines), indicating good agreement between the two measurement methods across the observed concentration range.

https://doi.org/10.1021/acssensors.6c02083
ACS Sens. XXXX, XXX, XXX−XXX

each blood draw, the coordinator collected the EDTA vacutainer tube containing blood and placed the tube in a wet ice bath for transportation to the laboratory for processing. The EDTA tubes were centrifuged for 10 min at 3000 revolutions per minute (rpm) at 4 degrees Celsius. The plasma was then pipetted into polypropylene tubes labeled with the corresponding collection time point and immediately placed on dry ice. Once all blood samples had been collected from the participant, the plasma samples were placed into the −80-degree Celsius freezer for subsequent shipment in batches for batch shipments, the polypropylene tubes containing

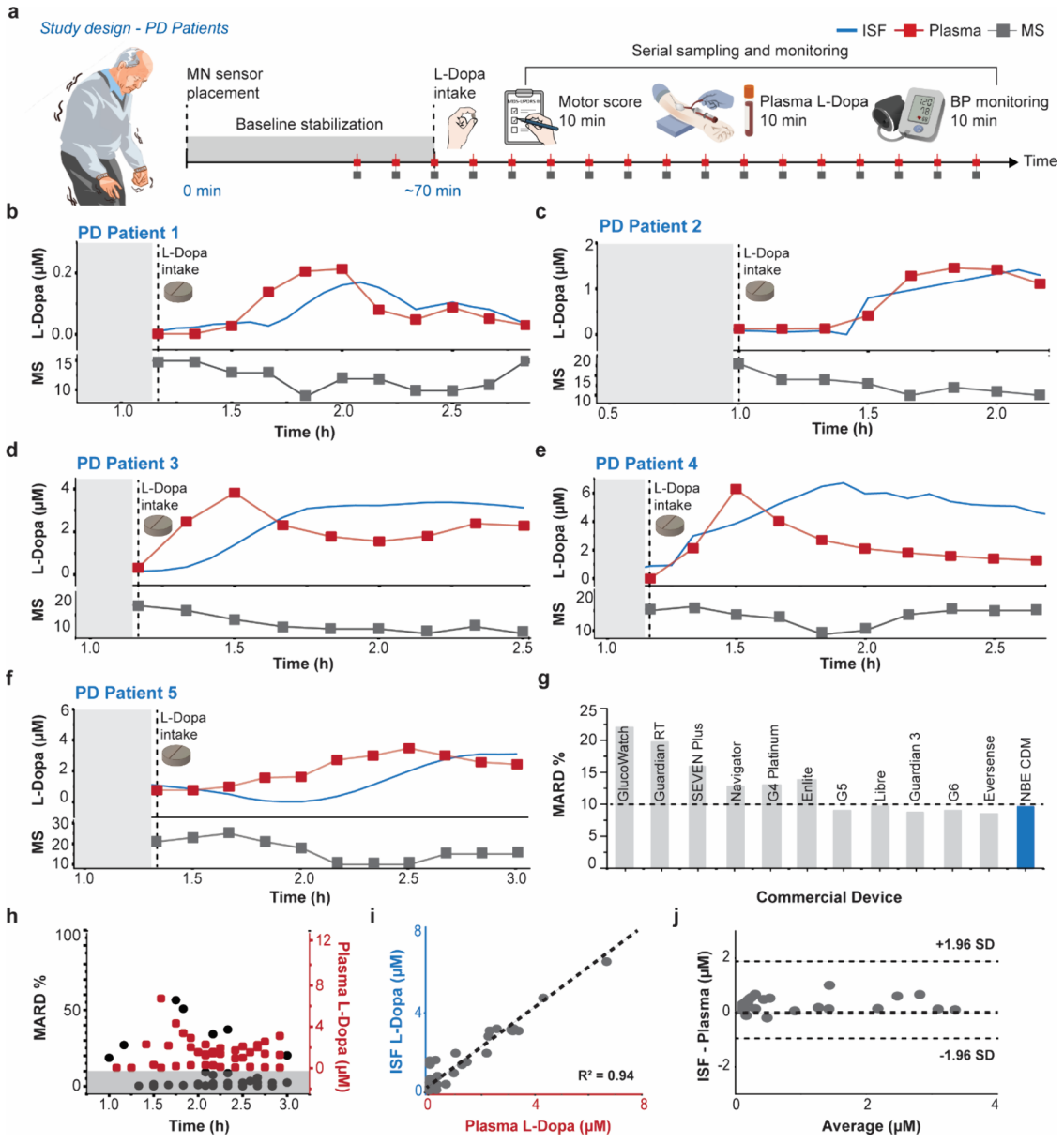

Figure 5. On-body monitoring of L-Dopa dynamics using a wearable MN device in participants with PD. (a) Experiment workflow used for evaluating the wearable MN sensor in participants with PD. L-Dopa$_{ISF}$ monitoring begins with a stabilization period to ensure a steady baseline signal. In parallel, L-Dopa$_{Plasma}$ monitoring is performed through venous blood draw performed every 10 min along with motor score evaluation. After baseline stabilization, subjects take a dose of oral carbidopa/L-Dopa immediate release in a 1:4 ratio. Throughout the study, blood pressure (BP) was measured every 10 min. (b−f) Real time profiles of L-Dopa concentrations measured in ISF using the MN device (blue) and in plasma using HPLC (red), and the motor scores from five PD patients. Oral administration of carbidopa/L-Dopa was performed following a stabilized period, indicated by the grey-shaded region. (g) MARD % values comparison between NBE CDM vs commercial CGMs. (h) Representative of MARD percentages and corresponding plasma L-Dopa concentrations during the study from all PD patients. MARD % values are shown as individual data points (black circles, left axis), plasma L-Dopa concentrations (μM) are overlaid (red squares, right axis), the behavior trend between both is observed. Most MARD % values remain below 10% (gray area), with occasional higher deviations, indicating overall good agreement between the MNs measurements and reference plasma levels across all subjects. (i) Correlation between ISF L-Dopa concentrations obtained via the MN device and corresponding plasma concentrations measured by HPLC across all subjects. A strong linear relationship ($R^2 = 0.94$) was observed, calculated upon applying delay-time correction. (j) Bland−Altman analysis comparing L-Dopa concentrations measured in ISF and plasma. The plot shows the mean difference (dashed line) and the ±1.96 SD limits of agreement (solid red lines), indicating good agreement between the two measurement methods across the observed concentration range.

https://doi.org/10.1021/acssensors.6c02083
ACS Sens. XXXX, XXX, XXX−XXX

plasma were placed into a 95kPa biohazard bag with absorbent pouches. Four lbs. of dry ice was placed at the bottom of the insulated container in a medium-sized insulated frozen shipping box. The sealed 95 kPa biohazard bag was placed on top of the dry ice, and an additional 10 lbs. of dry ice was placed on top of the sealed samples before sealing the box for shipment.

Plasma L-Dopa Concentration Analysis

Plasma samples were analyzed at the HPLC Bioanalytical Core at the Emory University School of Medicine, and prepared and analyzed as described below.

Sample Preparation. The plasma samples were thawed and sonicated with cup horn with pulse 2 s on 10 s off, an amplitude 50% for 5 min at 4 °C (QSONIC Q500A, Newtown CT). 450 μL of the plasma was mixed with 50 μl of 4 N percholoric acid and rested on ice for 15 min. The samples were centrifuged at 13,000 × *g* for 15 min at 4 °C to remove the precipitated proteins. The supernatants were transferred into fresh 0.22 μM PVDF microcentrifuge filter tubes. Any remaining particulate matter was eliminated by filtration through the spin filter at 5000 × *g* for 5 min at 4 °C. L-Dopa was measured in the supernatant.

HPLC Method. Monoamine were measured by ACQUITY ARC system equipped with a 3465 electrochemical detector (Waters). Separations were performed at 37 °C using an Xbridge BEH C18, 2.5 μm, 3 × 150 mm column (Waters). The mobile phase consisted of 100 mM citric acid, 100 mM phosphoric acid, pH 3.1, 0.1 mM EDTA, 950 mg/L 1-octanesulfonic acid, 5% acetonitrile. The detection flow cell was SenCell with 2 mm GC WE and the cell potential were set at 650 mV with salt bridge reference electrode. AST position was set at 1. ADF was 0.5 Hz. The needle was washed with water. Pump piston was washed with 15% isopropanol. A 10 μL of sample was injected. The samples were eluted isocratically at 0.6 mL/min. The analytes were identified by the matching criteria of retention time measures to known standards (Sigma Chemical Co., St. Louis MO). Compounds were quantified by comparing peak areas to those of standards.

Data Processing – Current to Concentration

Profiles of ISF L-Dopa current signals obtained from the wearable microneedle sensor and plasma L-Dopa concentrations measured by HPLC in healthy participants and those with PD were used for individualized calibration and translation of ISF signals to concentrations. For each participant, the maximum ISF L-Dopa current signal and maximum plasma L-Dopa concentration after pill administration were identified. Baseline-subtracted changes were calculated according to eqs 1 and 2:

$$\Delta I_{ISF} = I_{max} - I_0 \tag{1}$$

$$\Delta[\mathrm{L-Dopa}]_{Plasma} = [\mathrm{L-Dopa}]_{max} - [\mathrm{L-Dopa}]_0 \tag{2}$$

where baseline values (0) represent the stabilized signal or concentration prior to L-Dopa administration. Also, ΔI_{ISF} represents the difference current value obtained from the MN device, which is the subtraction of the current value at time zero (I_0) from the maximum current value (I_{max}) (Figure 3a). For the L-Dopa concentration difference ($\Delta[\mathrm{L\text{-}Dopa}]_{Blood}$), $[\mathrm{L\text{-}Dopa}]_{max}$ represents the highest L-Dopa concentration in plasma and $[\mathrm{L\text{-}Dopa}]_0$ indicates the L-Dopa concentration at time zero.

The ratio (a) between ΔI_{ISF} and $\Delta[\mathrm{L\text{-}Dopa}]_{Plasma}$ was then determined by (eq 3):

$$\frac{\Delta I\ ISF}{\Delta[\mathrm{L-Dopa}]\ \mathrm{Plasma}} = a\ (\mu\mathrm{A}\ \mu\mathrm{M}^{-1}) \tag{3}$$

where a is the subject-specific calibration ratio factor, accounting for inter-individual variability in skin permeability, tissue diffusion, and sensor response (Figure 3b). Using a, ISF current responses were translated into concentrations according to eq 4:

$$[\mathrm{L-Dopa}]_{ISF} = \frac{i\ ISF - i\ ISF\ baseline}{a} \tag{4}$$

where I_{ISF} is the real time current and $I_{ISF\ baseline}$ is the baseline current (Figure 3c,d).

A temporal lag between the ISF and plasma L-Dopa pharmacokinetics is expected due to diffusion from the vascular to the interstitial compartment.[41] A lag time (Δt) correction was thus applied. The lag time was calculated using eq 5:

$$\Delta t\ (\mathrm{min}) = t_{Plasma} - t_{ISF} \tag{5}$$

where t_{ISF} and t_{Plasma} represent the times of maximum ISF and plasma concentrations, respectively. Each ISF profile was shifted backward by the calculated lag time before correlation analysis (Figure 3e–g). After this shift, only the overlapping portions of the ISF and plasma profiles were retained for analysis (Figure 3h). L-Dopa plasma concentration points without corresponding ISF current values (i.e., data falling outside the overlap window after shifting) were excluded (Supporting Information Figures 10 and 11). The correlation between ISF-derived concentrations and plasma HPLC concentrations was then evaluated using Pearson correlation, Bland–Altman analysis and mean absolute relative difference (MARD). All calculations were processed using a custom Python script.

Mean Absolute Relative Difference (MARD) Calculation

The mean absolute relative difference (MARD) is a standard analytical metric used to evaluate the accuracy of continuous glucose monitoring (CGM) systems.[42−44] In this work, we adopted the same principle to assess the performance of our CDM microneedle sensor. A MARD value below 10% is typically considered acceptable for CGM systems. The MARD value of the present CDM device was calculated from paired measurements obtained in PD patients, where L-Dopa concentrations measured by the CDM sensor were compared with reference values obtained by HPLC, according to the following equation:

$$MARD = \frac{1}{n}\Sigma\left|\frac{CDM - HPLC}{HPLC}\right| \times 100 \tag{6}$$

Where CDM are the L-Dopa values obtained from our microneedle device paired to L-Dopa HPLC values from plasma samples. The calculated MARD for our device was 9.68%, demonstrating reasonable accuracy and stability for a first-generation CDM device deployed in a clinical study (Figure 5g,h).

RESULTS AND DISCUSSION

In Vitro Evaluation of the L-Dopa Microneedle Sensor

In this section, we evaluate the developed L-Dopa MN sensing platform; (Figure 2a) shows the reagent layer configuration on the Pt MN working electrode. A platinum nanoparticle (Pt NP) layer was electrodeposited to enhance electrical conductivity, biocompatibility, and electroactive surface area.[45] This layer supported the immobilization of tyrosinase (Tyr), followed by protective Nafion and PVC films. The enzymatic reaction between Tyr and L-Dopa produces L-Dopaquinone, which is electrochemically detected at a negative potential. To optimize the amperometric setup, the influence of the applied potential was evaluated over the 0.0 to −0.4 V range vs Ag/AgCl (Figure 2b and Supporting Information Figure 3a). Although higher negative potentials increased the L-Dopa signal, simultaneous O_2 reduction at −0.4 V compromised reliability.

https://doi.org/10.1021/acssensors.6c02083
ACS Sens. XXXX, XXX, XXX–XXX

Therefore, −0.3 V was selected as the optimal potential, providing sufficient sensitivity while minimizing background interference. L-Dopa calibration, carried out at −0.3 V and in PBS containing 10−80 μM L-Dopa (10 μM intervals) produced a linear response ($y = 0.0026x - 0.0019$, $R^2 = 0.9979$) (Supporting Information Figure 3b,c). Similarly, calibration in artificial interstitial fluid (ISF) with 5−50 μM L-Dopa (5 μM intervals) showed a linear range ($y = 0.0094x$-0.019, $R^2 = 0.998$) and LOD of 0.58 μM (at 3 S_d/m) (Figure 2c). These results confirm that the sensor sensitivity and linearity are suitable for detecting L-Dopa within the therapeutic range in ISF. The selectivity was assessed in artificial ISF spiked with 10 μM L-Dopa against physiologically relevant interferents, including ascorbic acid, acetaminophen, dopamine, glucose, lactic acid, tyrosine, and uric acid. Carbidopa typically co-administered with L-Dopa at a 1:4 ratio (2.5 μM Carbidopa: 10 μM L-Dopa), was also tested (Figure 2d and Supporting Information Figure 3d). The MN sensor showed high selectivity for L-Dopa, reflecting the specificity of TYR and the permselective properties of the Nafion and PVC films. Operational stability was evaluated in artificial ISF containing 10 μM L-Dopa at 5-min intervals over 580 min (~9.7 h). The current remained highly stable within 8.03% variation over the entire stability test period (Figure 2e and Supporting Information Figure 2e), owing to the protective anti-biofouling PVC film and effective crosslinking of TYR on the Pt NP-modified surface.[45,46] The storage stability was evaluated over a 10-day period at 4 °C. As shown in Figure 2f, the normalized current responses remained relatively stable, with fluctuations ranging from −7.47% to +16.66% compared to the baseline (day 0). These data demonstrate that the MN sensor maintained its functional integrity during the study period. These findings highlight that the MNs preserve reliable performance for at least 10 days, a relevant timeframe for laboratory testing, shipping, or short-term clinical use. To evaluate the reproducibility of the fabrication and modification processes, electrochemical signals were recorded from eight independently prepared MN sensors (Figure 2g). The sensors yielded highly reproducible current signals with minimal variations across different MNs devices, consistency between batch-to-batch modified MNs. The calculated relative standard deviation (RSD) of 5.99% confirms the robustness of the surface modification method. To verify robustness for wearable applications, the sensor performance was tested before and after skin insertion (Figure 2h). Ten insertions resulted in only a 4.76% signal decrease, confirming durability for single-use applications. While the performance declined slightly after 20 insertions, this is not a practical limitation since wearable sensors are intended for one-time use. The effect of physiological pH variability was also examined. The sensor was tested in artificial ISF at pH 6.5, 7.0, and 7.4 (Figure 2i). Signals increased slightly at acidic pH (10.64% at 6.5 and 4.04% at 7.0), reflecting protonation-dependent changes in L-Dopa. Overall, the in vitro characterization of the MN L-Dopa biosensor demonstrates that these sensor strips offer high sensitivity, selectivity, stability, and robustness. Notice that the in-vitro performance metrics fall within clinically relevant ranges, suggesting feasibility for patient monitoring.

Data Processing: Translating ISF L-Dopa Current Signals into Plasma L-Dopa Concentrations via Correlation with Plasma HPLC Measurements

A single-point calibration approach was used in the present work to account for inter-individual variability while enabling quantitative translation of ISF electrochemical current signals into equivalent plasma L-Dopa concentrations. To establish this calibration, the wearable MN sensor outputs were correlated with the plasma L-Dopa levels measured by HPLC in both healthy subjects and PD patients. For each participant, the peak ISF current response and the corresponding maximum plasma L-Dopa concentration following oral drug administration were identified. Baseline values were subtracted to obtain net peak responses (Figure 3a). The ratio between these corrected peak values defined the subject-specific calibration coefficient (a), as shown in Figure 3b. This coefficient accounts for inter-individual variability in skin permeability and tissue diffusion. Using this coefficient, ISF current values were converted to L-Dopa concentration in real time according to eq 3, described in the Methods section (Figure 3c,d). Considering the inherent pharmacokinetic delay between systemic circulation and ISF, a temporal correction factor (Δt) was computed as the time difference between the plasma and ISF L-Dopa peak occurrences. This delay was subsequently applied to temporally align both datasets (Figure 3e−g). Only the overlapping time segments of ISF and plasma concentration profiles were used for statistical analysis (Figure 3h). Importantly, although the peak ISF current response and peak plasma L-Dopa concentration were used to derive the subject-specific calibration coefficient, validation of the MN sensor did not rely on a single blood measurement. After application of the calibration coefficient and lag-time correction, all available HPLC plasma L-Dopa concentration points within the overlapping time window were used for comparison with the corresponding ISF L-Dopa profile. This approach enabled evaluation of the complete concentration-time profile rather than an agreement at a single calibration point.

Prior to correction, the ISF signals (blue) displayed a consistent delay relative to plasma L-Dopa concentrations (red). Following the application of the subject-specific Δt adjustment, calculated from the time-to-maximum concentration difference, the ISF profiles were shifted to align with their corresponding plasma L-Dopa profiles. After the profiles alignment, ISF and plasma L-Dopa trajectories displayed a rise and decay kinetics in both healthy and PD participants. This temporal and quantitative calibration demonstrates the feasibility of real-time monitoring of plasma L-Dopa dynamics through the MN ISF electrochemical sensing, towards capturing individual pharmacokinetic variations with high fidelity. Lag time corrections across all subjects are provided in Supporting Information Figures 10 and 11.

On-Body Monitoring of L-Dopa via a Wearable MN Device in Healthy Subjects

Before testing the device in participants with PD, the MN-based CDM device was evaluated in healthy subjects after ingestion of fava beans (Supporting Information Table 2), which provide a natural dietary source of L-Dopa.[47,48] This non pharmaceutical model provides a safe and physiologically relevant means to validate the device's capability to detect dynamic changes in L-Dopa concentrations. In this preliminary study, healthy volunteers wore the CDM device for approximately 2−3 h (following the UCSD IRB Project #171927), according to the process described in the Methods section: Microneedle Sensor Testing in Healthy Subjects after Fava Bean Consumption. The ISF current signal was continuously recorded using chronoamperometry at −0.3 V. As shown in Supporting Information Figure 5, the CDM device successfully tracked

https://doi.org/10.1021/acssensors.6c02083
ACS Sens. XXXX, XXX, XXX−XXX

temporal fluctuations in L-Dopa following fava bean ingestion in the six participants, with an average ISF delay of approximately 20 min relative to the changing capillary blood levels. Peak L-Dopa concentrations varied among individuals, reflecting physiological differences in gastrointestinal absorption, metabolic rate, as well as other dietary factors. Overall, these results demonstrate that the CDM device can reliably detect dynamic changes in L-Dopa in human participants, supporting its readiness for further validation under standardized pharmaceutical conditions.

To further assess performance, three additional healthy subjects (Supporting Information Table 3) were recruited to monitor L-Dopa kinetics following administration of oral carbidopa/L-Dopa pills. All visits followed the process described in the Methods section: Testing in Healthy Subjects after Ingestion of the Oral Carbidopa/L-Dopa Immediate-Release Tablet. The ISF currents were continuously measured at −0.3 V. After baseline stabilization for approximately 90 min, each subject ingested one oral tablet containing immediate-release carbidopa/L-Dopa 25 mg/100 mg. Venous blood samples were collected every 10 min by nursing staff (Figure 4a), processed, and sent for HPLC-based L-Dopa concentration analysis, following the process described in the Methods section: Plasma L-Dopa Concentration Analysis. Vital signs, including heart rate and blood pressure, were recorded at the same intervals (Supporting Information Figure 6). Both ISF and plasma L-Dopa trends exhibited the expected pharmacokinetic increases following medication ingestion, confirming the device's ability to capture dynamic L-Dopa profiles. The participants displayed ISF responses with subject-specific lag times of 20, 65, and 30 min, consistent with expected interstitial-blood diffusion delays (Figure 4b−d). Correlation analysis between ISF and plasma L-Dopa concentrations revealed a positive linear relationship with a $R^2 = 0.83$, r = 0.91 (Figure 4e), and confirmed that this relationship was highly significant between both methods ($p < 0.001$) after correcting for time delays. Additionally, Bland-Altman analysis demonstrated an acceptable agreement between the two methods, with an average concentration difference of 1.29 and a standard deviation (SD) of 3.74, falling within the limits of agreement from −6.04 to 8.62 (±1.96 SD), indicating consistency across the concentration range (Figure 4f). After the device was removed from the body, transient MN marks were visible on the skin but disappeared completely within 30 min (Supporting Information Figure 12a−c). Collectively, these findings confirm that the wearable MN-based CDM device accurately reflects pharmacokinetic changes following both dietary and pharmaceutical L-Dopa administration in healthy participants. The close correlation with HPLC L-Dopa measurements and the continuous detection of concentration dynamics support the potential utility of the MN CDM strategy for personalized therapeutic monitoring in PD management.

On-Body Monitoring of L-Dopa Using the Wearable MN Device in Participants with Parkinson's Disease

The developed MN sensors were subsequently critically evaluated in clinical settings through testing in participants with PD along with simultaneous motor score assessment and blood pressure measurements. This study aimed to evaluate the capability of the MN sensor to continuously and accurately monitor ISF L-Dopa levels and to assess their relationship with blood L-Dopa concentrations and motor symptom responses. Seven patients with PD were recruited for this pilot study; however, data from only five participants are presented, as the testing was terminated early for two participants due to events unrelated to device performance (Supporting Information Figure 13). All study visits followed the process described in the Methods section: Testing in Participants with PD after Ingestion of Oral Carbidopa/L-Dopa Immediate-Release Tablets (Figure 5a and Supporting Information Figure 14). Figure 5b−f illustrates the relationship between L-Dopa concentration in ISF and plasma, along with the motor score response among the five PD patients. In all cases, we observed the expected rising plasma and ISF L-Dopa concentrations after medication administration, with varying individual delay times in the L-Dopa ISF profiles compared to plasma L-Dopa levels in each participant. Similar time delays are commonly observed using commercial CGM systems for the management of diabetes.[49] As expected, the temporal L-Dopa ISF profiles correlated closely with the motor responses, with rising L-Dopa levels corresponding to lower motor scores, reflecting improvements in motor symptoms.

Among all five participants, PD Patient 1 (Figure 5b) presented the lowest L-Dopa levels in both plasma and ISF profiles. Despite of these relatively low levels, the MN sensor reliably measured L-Dopa ISF concentrations in close agreement with HPLC plasma measurement, with an approximate 10-minute lag and a closely matching temporal profile. In contrast, while the L-Dopa levels of PD Patient 2 started to increase ∼30 min after the pill intake, a shorter delay time (∼10 min) was observed between the plasma and ISF L-Dopa measurements. Similarly, motor score improvements began 10 min after taking the pill. (Figure 5c). Such reduced delay indicates faster peripheral distribution or increased tissue permeability, leading to a quicker pharmacodynamic response. For both PD Patients 3 and 4, the plasma L-Dopa concentration began to rise rapidly within 10 min after the pill intake, reaching highest levels at 20 min (Figure 5d,e). The corresponding ISF signals increased more slowly, reaching their maximum values at 35 and 40 min, respectively. The ISF profiles of PD Patients 3 and 4 correlated closely with the corresponding trends in the motor score response (Figure 5d,e). In PD Patient 5, plasma L-Dopa concentration increased slowly after the pill intake, followed by a slow rise of ISF levels (measured by the MN sensor), with a 40 min delay time between blood and ISF (Figure 5f).

In addition to the strong agreement between plasma and ISF L-Dopa levels, the MN sensor successfully captured fluctuations in the ISF profile that mirrored the dynamic changes observed in plasma L-Dopa concentrations, demonstrating its capability to track real-time pharmacokinetic variability, all with an average delay time of 15 min to reach L-Dopa ISF maximum concentration across subjects. Additionally, motor scores followed the expected inverse trend, aligning with both plasma and ISF profiles, whereby the patient's motor function improved as L-Dopa concentrations increased. These findings from PD patients collectively provide pilot data supporting the performance of the developed MN sensor, highlighting its sensitivity, temporal resolution, and capability to accurately reflect both pharmacokinetic and pharmacodynamic responses, even at low analyte concentrations, along with correlation to corresponding motor scores.

The calculated MARD for our device was 9.68%, demonstrating good accuracy and stability for a first-generation CDM device deployed in a clinical pilot study (Figure 5h). As illustrated in Figure 5g, such low MARD compares favorably to those of commercial continuous glucose monitoring systems.[50] The correlation between the L-Dopa ISF and plasma

https://doi.org/10.1021/acssensors.6c02083
ACS Sens. XXXX, XXX, XXX−XXX

concentrations was calculated across all subjects (after time-delay corrections were applied), leading to a positive linear relationship of $R^2 = 0.94$, r = 0.97 (Figure 5i). The linear regression analysis confirmed that this relationship was highly significant ($p < 0.001$), with a slope close to unity, indicating good proportional agreement, although a small systematic bias was observed. Bland−Altman analysis revealed a mean difference of 0.12 with 95% limits of agreement ranging from −1.65 to 1.91, indicating that most differences between the two methods fall within this range. These findings suggest that ISF measurements have potential to monitor L-Dopa dynamics relative to plasma concentrations (Figure 5j). In this context, the mean difference represents systematic bias between methods, while the ±1.96 standard deviation (SD) defines the limits within which 95% of the differences between ISF and plasma L-Dopa measurements are expected to lie, supporting method comparability. The observed variability within the limits of agreement may partially arise from physiological differences in L-Dopa transport between plasma and ISF. To account for inter-subject variability, the temporal lag (Δt) between plasma and ISF profiles was not fixed across all participants. Instead, Δt was determined individually for each subject based on the difference between the plasma and ISF peak times, and the corresponding ISF profile was shifted prior to comparison (Figure 3e−h). Therefore, subject-specific lag effects were incorporated into the analysis. No clear concentration-dependent trend in the Bland−Altman residuals was observed in the current dataset. However, the sample size was not sufficient to systematically evaluate whether Δt varies with L-Dopa concentration or other physiological factors. Future studies involving larger cohorts and higher temporal resolution measurements will be valuable for investigating potential concentration-dependent or physiological influences on the lag time and improving further the agreement between ISF and plasma measurements. After the CDM device removal, we observed small skin indentations from the microneedles on the subject's arm, which disappeared in less than 30 min (Supporting Information Figure 12d−h). This observation confirms the minimally invasive nature and favorable biocompatibility of the MN device.

Feedback from participants with PD on their perception of the MN device was collected using a five-point Likert scale, with responses coded numerically from 1 (strongly disagree) to 5 (strongly agree), as summarized descriptively by item (Supporting Information Figure 15), with an average acceptance of 4.5 over 5 in the Likert scale. Post-use questionnaire data from the PD participants supported the high acceptability of the MN platform; 100% strongly agreed that they would use it at home or in public, 100% agreed or strongly agreed that the device was comfortable, did not irritate skin, and would not interfere with activities, and 75% agreed or strongly agreed that the device was discreet and easy to use (25% neutral). Overall, the results from participants with PD demonstrate the capacity of the MN sensor to reflect pharmacokinetic changes following oral L-Dopa ingestion and demonstrate its potential utility in clinical settings for eventual personalized patient monitoring. This study thus supports the feasibility of MN-based ISF sensing as a reliable continuous, real-time L-Dopa monitoring tool that would pave the way for closed-loop systems for personalized PD management.

■ CONCLUSIONS

Despite major efforts to develop L-Dopa detection technologies, no MN devices have yet progressed to human clinical trials, representing a critical translational gap that limits practical validation of MN platforms and the development of closed-loop systems to improve PD management. To address this gap, we introduce a MN-based sensing platform and demonstrate, for the first time, its application for CDM in both healthy human volunteers and participants with PD in a clinical setting. Such a minimally invasive, wearable MN-based biosensor utilizes a tyrosinase-functionalized working electrode to detect L-Dopa in ISF via enzymatic electrochemical sensing. The device was evaluated in healthy subjects and PD patients, with ISF signals validated against plasma L-Dopa concentrations measured by HPLC. Using subject-specific calibration and lag-time correction, ISF-derived profiles showed strong agreement with plasma pharmacokinetics, and an inverse relationship was observed between L-Dopa levels and motor scores. The estimated ISF L-Dopa levels correlated with HPLC-based plasma measurements and corresponding motor response profiles. These correlations support the potential clinical relevance of continuous monitoring for assessing therapeutic response, while demonstrating the safety and tolerability of the device in human subjects.

Overall, this pilot study presents the first human clinical validation of a MN-based system for continuous L-Dopa monitoring, demonstrating its ability to capture subject-specific pharmacokinetic fluctuations in both PD patients and healthy participants. The current reliance on subject-specific calibration and lag-time correction represents a limitation of this pilot study. The relatively small number of participants, particularly those with PD, limits our ability to establish generalized calibration models and standardized lag-time correction approaches. Larger clinical studies will be required to investigate the feasibility of multi-point calibration methods, better characterize inter-patient variability, evaluate long-term reliability, and determine the clinical utility of continuous L-Dopa monitoring for treatment optimization and clinical decision-making. Such studies will also provide the datasets necessary to develop population-based calibration strategies, automated lag-time correction algorithms, and potentially develop artificial intelligence (AI)-assisted predictive models that could further improve calibration accuracy and eventually eliminate the need for extensive subject-specific calibration while maintaining individualized accuracy.

While the present work was limited by a modest sample size, a short monitoring duration due to device's battery life, and the need for subject-specific calibration, these findings demonstrate the clinical feasibility of the MN CDM system and highlight the tremendous potential of the wearable MN platform. In this pilot study, the optimized wearable system provided approximately 6 h of continuous operation, which was sufficient to capture the pharmacokinetic window following a single L-Dopa administration. However, real-world clinical implementation and routine PD management will require extended monitoring over an entire day and across multiple dosing cycles to enable continuous assessment of medication levels and support personalized dose optimization by patients and healthcare providers.

Another important consideration for real-world deployment is the potential effect of co-administered PD medications and other electroactive constituents on sensor performance. In the present study, participants with PD received immediate-release oral carbidopa/L-Dopa and were either no other antiparkinsonian medications or taking stable doses of such medications. In addition, participants underwent a medication washout period of at least 10 h before testing and were instructed to

https://doi.org/10.1021/acssensors.6c02083
ACS Sens. XXXX, XXX, XXX−XXX

avoid caffeine and high-protein foods to minimize potential effects on the HPLC analysis and L-Dopa bioavailability, respectively. Although the sensor displayed good agreement with HPLC measurements under these controlled conditions, further investigations involving larger and more diverse patient populations will be necessary to fully assess the sensor's specificity, calibration robustness, long-term clinical performance, and wearability. Particular attention should be given to potential sources of variability, including co-administered medications, additional electroactive metabolites, skin conditions, change in enzyme activity during prolonged use, variations in ISF turnover rates, inflammatory responses, tissue reactions, and long-term signal drift. Future studies involving extended wear durations should therefore incorporate comprehensive assessments of device safety and performance, including analyses of inflammatory biomarkers, and tissue histology, evaluation of enzyme stability, and characterization of long-term signal stability under real-world conditions.

Future work should focus on conducting larger and longer-term clinical studies, improving device stability and battery life, reducing the need for subject-specific calibration, expanding interference assessments, and integrating additional physiological sensors and motor symptom monitoring to provide a more comprehensive assessment of each patient's condition. In addition, incorporating AI and predictive modeling could enable individualized interpretation of continuous L-Dopa data, support dose optimization, anticipate motor fluctuations, and ultimately facilitate closed-loop therapeutic systems towards personalized PD management, thereby minimizing motor fluctuations, improving quality of life, and reducing healthcare burden.

■ ASSOCIATED CONTENT

Data Availability Statement

The code for the translation of ISF L-Dopa current signals (μA) into ISF L-Dopa concentrations (μM), MARD calculation, and time delay adjustment is available via GitHub at: https://github.com/umahmood351/microneedles-wang-ldopa.git.

Supporting Information

The Supporting Information is available free of charge at https://pubs.acs.org/doi/10.1021/acssensors.6c02083.

PD patients' and healthy subjects' information, development of the microneedle sensor device, SEM images, in vitro characterization, in vitro cytotoxicity assessment, on-body monitoring, motor function analysis, motion test effect study, time delay adjustment, pictures of the microneedles array insertion mark, PD patient's clinic diagram, L-Dopa monitoring general set-up, and post-use questionnaire responses (DOCX)

■ AUTHOR INFORMATION

Corresponding Authors

Irene Litvan – *Department of Neurosciences, University of California San Diego, La Jolla, California 92093, United States;* Email: ilitvan@ucsd.edu

Joseph Wang – *Aiiso Yufeng Li Family Department of Chemical and Nano Engineering, University of California San Diego, La Jolla, California 92093, United States;* orcid.org/0000-0002-4921-9674; Email: josephwang@ucsd.edu

Authors

Maria Reynoso – *Aiiso Yufeng Li Family Department of Chemical and Nano Engineering, University of California San Diego, La Jolla, California 92093, United States*

Chochanon Moonla – *Aiiso Yufeng Li Family Department of Chemical and Nano Engineering, University of California San Diego, La Jolla, California 92093, United States;* orcid.org/0000-0001-5885-1244

Katherine Longardner – *Department of Neurosciences, University of California San Diego, La Jolla, California 92093, United States*

Nuenghathai Chaiya – *Aiiso Yufeng Li Family Department of Chemical and Nano Engineering, University of California San Diego, La Jolla, California 92093, United States*

Stacey Surace – *Shu Chien - Gene Lay Department of Bioengineering, University of California San Diego, La Jolla, California 92093, United States*

An-Yi Chang – *Aiiso Yufeng Li Family Department of Chemical and Nano Engineering, University of California San Diego, La Jolla, California 92093, United States*

Tamoghna Saha – *Aiiso Yufeng Li Family Department of Chemical and Nano Engineering, University of California San Diego, La Jolla, California 92093, United States*

Umair Mahmood – *Shu Chien - Gene Lay Department of Bioengineering, University of California San Diego, La Jolla, California 92093, United States*

Muhammad Khan – *Aiiso Yufeng Li Family Department of Chemical and Nano Engineering, University of California San Diego, La Jolla, California 92093, United States*

Michael Skipworth – *Department of Neurosciences, University of California San Diego, La Jolla, California 92093, United States*

Ian McGregor – *Aiiso Yufeng Li Family Department of Chemical and Nano Engineering, University of California San Diego, La Jolla, California 92093, United States*

Ava Van Damme – *Shu Chien - Gene Lay Department of Bioengineering, University of California San Diego, La Jolla, California 92093, United States*

Lidia F. Vazquez – *Shu Chien - Gene Lay Department of Bioengineering, University of California San Diego, La Jolla, California 92093, United States*

Eshita Shah – *Department of Neurosciences, University of California San Diego, La Jolla, California 92093, United States*

Hao Luan – *Aiiso Yufeng Li Family Department of Chemical and Nano Engineering, University of California San Diego, La Jolla, California 92093, United States*

Complete contact information is available at: https://pubs.acs.org/doi/10.1021/acssensors.6c02083

Author Contributions

[+]M.R., C.M., and K.L. contributed equally to this work.

Notes

The authors declare no competing financial interest.

■ ACKNOWLEDGMENTS

This work was supported by the UCSD Center for Wearable Sensors (CWS). N.C. would like to thank the National Research Council of Thailand (NRCT) (contract no. N41A650115) for a

PhD Fellowship, Maejo University. The plasma samples analysis was supported by the Emory HPLC Bioanalytical Core (RRID:SCR_023531). This publication was supported in part by the Altman Clinical and Translational Research Institute at the University of California, San Diego, funded by the National Center for Advancing Translational Sciences, National Institutes of Health, Award Number UM1TR005449. The content is solely the responsibility of the authors and does not necessarily represent the official views of the NIH. This manuscript is subject to the NIH Public Access Policy, and the final peer-reviewed manuscript will be made publicly available in PubMed Central upon the official date of publication.

REFERENCES

(1) Jellinger, K. A. Parkinson's Disease. In *Neurodegeneration: The Molecular Pathology of Dementia and Movement Disorders*; Dickson, D. W., Weller, R. O., Eds.; Wiley-Blackwell: **2011**, pp 194–223.

(2) Willis, A. W.; Roberts, E.; Beck, J. C.; Fiske, B.; Ross, W.; Savica, R.; Van Den Eeden, S. K.; Tanner, C. M.; Marras, C. Incidence of Parkinson Disease in North America. *NPJ Parkinsons Dis.* **2022**, *8*, 170.

(3) Patel, U. S.; Sufi, A. J.; Mehra, R. S.; Patel, A. S.; Noolvi, M. N.; Rathod, M. N. A newer approach to Parkinson's disease: Addressing therapeutic features, repurposing drugs and the latest concepts with future goals. *World J. Biol. Pharm. Health Sci.* **2025**, *21*, 568–588.

(4) Zuo, Y.; Ding, X.; Liu, Z.; Xie, Y.; Liu, G.; Liu, C. Diverse pathways for the treatment of Parkinson's disease: integration and development of traditional and emerging therapies. *Neuroscience* **2025**, *568*, 388–398.

(5) Goud, K. Y.; Moonla, C.; Mishra, R. K.; Yu, C.; Narayan, R.; Litvan, I.; Wang, J. Wearable electrochemical microneedle sensor for continuous monitoring of levodopa: toward Parkinson management. *ACS Sens.* **2019**, *4*, 2196–2204.

(6) Tenchov, R.; Sasso, J. M.; Zhou, Q. A. Evolving landscape of Parkinson's disease research: challenges and perspectives. *ACS Omega* **2025**, *10* (2), 1864.

(7) Prates-Rodrigues, M.; Schweizer, B. L. A.; de Paula Gomes, C.; Ribeiro, Â. M.; Padovan-Neto, F. E.; Masini, D.; Lopes-Aguiar, C. Challenges and opportunities in exploring non-motor symptoms in 6-hydroxydopamine models of Parkinson's disease: a systematic review. *J. Neurochem.* **2025**, *169*, No. e70008.

(8) Pringsheim, T.; Jette, N.; Frolkis, A.; Steeves, T. D. L. The prevalence of Parkinson's disease: a systematic review and meta-analysis. *Mov. Disord.* **2014**, *29*, 1583–1590.

(9) Foltynie, T.; Bruno, V.; Fox, S.; Kühn, A. A.; Lindop, F.; Lees, A. J.Medical, surgical, and physical treatments for Parkinson's disease. *Lancet* **2024**, *403* (10423), 305–324.

(10) Fang, L.; Ren, H.; Mao, X.; Zhang, S.; Cai, Y.; Xu, S.; Zhang, Y.; Li, L.; Ye, X.; Liang, B. Differential amperometric microneedle biosensor for wearable levodopa monitoring of Parkinson's disease. *Biosensors* **2022**, *12*, 102.

(11) Liu, X.; Zhang, Y.; Weng, Y.; Zhong, M.; Wang, L.; Gao, Z.; Hu, H.; Zhang, Y.; Huang, B.; Huang, R. Levodopa therapy affects brain functional network dynamics in Parkinson's disease. *Prog. Neuro-Psychopharmacol. Biol. Psychiatry* **2025**, *136*, No. 111169.

(12) Probst, D.; Batchu, K.; Younce, J. R.; Sode, K. Levodopa: from biological significance to continuous monitoring. *ACS Sens.* **2024**, *9* (8), 3828.

(13) Feske, S. K. Pharmacology of commonly used drugs. In *Office Practice of Neurology*; Churchill Livingstone: **2003**, *2*, pp 225–238.

(14) Khor, S.-P.; Hsu, A. The pharmacokinetics and pharmacodynamics of levodopa in the treatment of Parkinson's disease. *Curr. Clin. Pharmacol.* **2007**, *2*, 234–243.

(15) Leta, V.; Klingelhoefer, L.; Longardner, K.; Campagnolo, M.; Levent, H. Ç.; Aureli, F.; Metta, V.; Bhidayasiri, R.; Chung-Faye, G.; Falup-Pecurariu, C.; Stocchi, F.; Jenner, P.; Ray Chaudhuri, K. Gastrointestinal barriers to levodopa transport and absorption in Parkinson's disease. *Eur. J. Neurol.* **2023**, *30* (5), 1465–1480.

(16) Poewe, W.; Mahlknecht, P. Pharmacologic treatment of motor symptoms associated with Parkinson disease. *Neurol. Clin.* **2020**, *38*, 255–267.

(17) Teymourian, H.; Tehrani, F.; Longardner, K.; Mahato, K.; Podhajny, T.; Moon, J.-M.; Kotagiri, Y. G.; Sempionatto, J. R.; Litvan, I.; Wang, J. Closing the loop for patients with Parkinson disease: where are we? *Nat. Rev. Neurol.* **2022**, *18*, 497–507.

(18) Lozano, A. M.; Lipsman, N.; Bergman, H.; Brown, P.; Chabardes, S.; Chang, J. W.; Matthews, K.; McIntyre, C. C.; Schlaepfer, T. E.; Schulder, M.; Temel, Y.; Volkmann, J.; Krauss, J. K. Deep brain stimulation: current challenges and future directions. *Nat. Rev. Neurol.* **2019**, *15*, 148–160.

(19) Zhou, Y. Z.; Alany, R. G.; Chuang, V.; Wen, J. Studies of the Rate Constant of l-DOPA Oxidation and Decarboxylation by HPLC. *Chromatographia* **2012**, *75*, 597–606.

(20) Li, S.-F.; Wu, H.-L.; Yu, Y.-J.; Li, Y.-N.; Nie, J.-F.; Fu, H.-Y.; Yu, R.-Q. Quantitative analysis of levodopa, carbidopa, and methyldopa in human plasma samples using HPLC-DAD combined with second-order calibration based on alternating trilinear decomposition algorithm. *Talanta* **2010**, *81*, 805–812.

(21) Yumoto, E.; Yanagihara, N.; Asahina, M. The simple and rapid quantification method for L-3,4-dihydroxyphenylalanine (L-DOPA) from plant sprout using liquid chromatography-mass spectrometry. *Plant Biotechnol.* **2022**, *39*, 199–204.

(22) Mahato, K.; Moon, J.-M.; Moonla, C.; Longardner, K.; Ghodsi, H.; Litvan, I.; Wang, J. Biosensor Strip for Rapid On-Site Assessment of Levodopa Pharmacokinetics along with Motor Performance in Parkinson's Disease. *Angew. Chem., Int. Ed.* **2024**, *63* (136), No. e202403583.

(23) Moon, J.-M.; Teymourian, H.; De la Paz, E.; Sempionatto, J. R.; Mahato, K.; Sonsa-ard, T.; Huang, N.; Longardner, K.; Litvan, I.; Wang, J. *Angew. Chem., Int. Ed.* **2021**, *60*, 19074.

(24) Teymourian, H.; Tehrani, F.; Mahato, K.; Wang, J. Lab under the Skin: Microneedle Based Wearable Devices. *Adv. Healthcare Mater.* **2021**, *10*, No. 2002255.

(25) Moonla, C.; Reynoso, M.; Chang, A.-Y.; Saha, T.; Surace, S.; Wang, J. Microneedle-Based Multiplexed Monitoring of Diabetes Biomarkers: Capabilities Beyond Glucose Toward Closed-Loop Theranostic Systems. *ACS Sens.* **2025**, *10* (8), 5363–5379.

(26) Mouradian, MM.; Junecos, JL.; Fabbrini, G.; Schlegel, J.; Bartko, J. J.; Chase, T. N. Motor fluctuations in Parkinson's disease: Central pathophysiological mechanisms, part II. *Ann. Neurol.* **1988**, *24* (3), 372–378.

(27) Nutt, J. G.; Woodward, W. R.; Hammerstad, J. P.; Carter, J. H.; Anderson, J. L. The "on-off" phenomenon in Parkinson's disease Relation to levodopa absorption and transport. *N. Engl. J. Med.* **1984**, *310* (8), 483–488.

(28) Mouradian, M. M.; Heuser, I. J.; Baronti, F.; Chase, T. N. Modification of central dopaminergic mechanisms by continuous levodopa therapy for advanced Parkinson's disease. *Ann. Neurol.* **1990**, *27* (1), 18–23.

(29) Chase, TN. The significance of continuous dopaminergic stimulation in the treatment of Parkinson's disease. *Drugs* **1998**, *55* (Suppl 1), 1–9.

(30) Nutt, J. G. Pharmacokinetics and pharmacodynamics of levodopa. *Mov. Disord.* **2008**, *23* (Suppl 3), S580–584.

(31) Teymourian, H.; Moonla, C.; Tehrani, F.; Vargas, E.; Aghavali, R.; Barfidokht, A.; Tangkuaram, T.; Mercier, P. P.; Dassau, E.; Wang, J. Microneedle-based detection of ketone bodies along with glucose and lactate: toward real-time continuous interstitial fluid monitoring of diabetic ketosis and ketoacidosis. *ACS Sens.* **2020**, *5*, 2291.

(32) Moonla, C.; Reynoso, M.; Casanova, A.; Chang, A.-Y.; Djassemi, O.; Balaje, A.; Abbas, A.; Li, Z.; Mahato, K.; Wang, J. Continuous Ketone Monitoring via Wearable Microneedle Patch Platform. *ACS Sens.* **2024**, *9* (2), 1004–1013.

(33) Reynoso, M.; Chang, A.-Y.; Wu, Y.; Murray, R.; Suresh, S.; Dugas, Y.; Wang, J.; Arroyo-Currás, N. 3D-Printed, Aptamer-Based Microneedle Sensor Arrays Using Magnetic Placement on Live Rats

https://doi.org/10.1021/acssensors.6c02083
ACS Sens. XXXX, XXX, XXX–XXX

for Pharmacokinetic Measurements in Interstitial Fluid. *Biosens. Bioelectron.* **2024**, *244*, No. 115802.
(34) Postuma, R. B.; Poewe, W.; Litvan, I.; Lewis, S.; Lang, A. E.; Halliday, G.; Goetz, C. G.; Chan, P.; Slow, E.; Seppi, K.; Schaffer, E.; Rios-Romenets, S.; Mi, T.; Maetzler, C.; Li, Y.; Heim, B.; Bledsoe, I. O.; Berg, D. Validation of the MDS clinical diagnostic criteria for Parkinson's disease. *Mov. Disord.* **2018**, *33* (10), 1601−1608.
(35) Postuma, R. B.; Berg, D.; Stern, M.; Poewe, W.; Olanow, C. W.; Oertel, W.; Obeso, J.; Marek, K.; Litvan, I.; Lang, A. E.; Halliday, G.; Goetz, C. G.; Gasser, T.; Dubois, B.; Chan, P.; Bloem, B. R.; Adler, C. H.; Deuschl, G. MDS clinical diagnostic criteria for Parkinson's disease. *Mov. Disord.* **2015**, *30* (12), 1591−1601.
(36) Hoehn, MM.; Yahr, MD. Parkinsonism: onset, progression and mortality. *Neurology* **1967**, *17* (5), 427.
(37) Emre, M.; Aarsland, D.; Brown, R.; Burn, D. J.; Duyckaerts, C.; Mizuno, Y.; Broe, G. A.; Cummings, J.; Dickson, D. W.; Gauthier, S.; Goldman, J.; Goetz, C.; Korczyn, A.; Lees, A.; Levy, R.; Litvan, I.; McKeith, I.; Olanow, W.; Poewe, W.; Quinn, N.; Sampaio, C.; Tolosa, E.; Dubois, B. Clinical diagnostic criteria for dementia associated with Parkinson's disease. *Mov. Disord.* **2007**, *22* (12), 1689−1707.
(38) Goldstein, D. S.; Stull, R.; Markey, S. P.; Marks, E. S.; Keiser, H. R. Dihydrocaffeic acid: a common contaminant in the liquid chromatographic-electrochemical measurement of plasma catecholamines in man. *J. Chromatogr.* **1984**, *311* (1), 148−153.
(39) Virmani, T.; Tazan, S.; Mazzoni, P.; Ford, B.; Greene, P. E. Motor fluctuations due to interaction between dietary protein and levodopa in Parkinson's disease. *J. Clin. Mov. Disord.* **2016**, *3* (1), 8.
(40) Goetz, C. G.; Tilley, B. C.; Shaftman, S. R.; Stebbins, G. T.; Fahn, S.; Martinez-Martin, P.; Poewe, W.; Sampaio, C.; Stern, M. B.; Dodel, R.; Dubois, B.; Holloway, R.; Jankovic, J.; Kulisevsky, J.; Lang, A. E.; Lees, A.; Leurgans, S.; LeWitt, P. A.; Nyenhuis, D.; Olanow, C. W.; Rascol, O.; Schrag, A.; Teresi, J. A.; van Hilten, J. J.; LaPelle, N. Movement Disorder Society-sponsored revision of the Unified Parkinson's Disease Rating Scale (MDS-UPDRS): scale presentation and clinimetric testing results. *Mov. Disord.* **2008**, *23* (15), 2129−2170.
(41) Friedel, M.; Thompson, I. A. P.; Kasting, G.; Polsky, R.; Cunningham, D.; Soh, H. T.; Heikenfeld, J. Opportunities and challenges in the diagnostic utility of dermal interstitial fluid. *Nat. Biomed. Eng.* **2023**, *7*, 1541−1555.
(42) Vigersky, R. A.; Shin, J. The Myth of MARD (Mean Absolute Relative Difference): Limitations of MARD in the Clinical Assessment of Continuous Glucose Monitoring Data. *Diabetes Technol. Ther.* **2024**, *26* (S3), 38.
(43) Reiterer, F.; Polterauer, P.; Schoemaker, M.; Schmelzeisen-Redecker, G.; Freckmann, G.; Heinemann, L.; Del Re, L. Significance and Reliability of MARD for the Accuracy of CGM Systems. *J. Diabetes Sci. Technol.* **2017**, *11* (1), 59−67.
(44) Yang, J.; Gong, X.; Zheng, Y.; Duan, H.; Chen, S.; Wu, T.; Yi, C.; Jiang, L.; Haick, H. Microneedle-Based Integrated Pharmacokinetic and Pharmacodynamic Evaluation Platform for Personalized Medicine. *Nat. Commun.* **2025**, *16*, 6260.
(45) Soni, K.; Korgaokar, S.; Kumar, N.; Bhardwaj, L.; Parmar, J.; Ameta, R. K. Recent advances in platinum nanoparticle-based electrochemical sensors and their applications. *Discov. Electrochem.* **2025**, *2*, 33.
(46) Ruiz-Valdepenas Montiel, V.; Sempionatto, J. R.; Esteban-Fernández de Ávila, B.; Whitworth, A.; Campuzano, S.; Pingarrón, J. M.; Wang, J. Delayed sensor activation based on transient coatings: Biofouling protection in complex biofluids. *J. Am. Chem. Soc.* **2018**, *140* (43), 14050−14053.
(47) Mehran, S. M. M.; B.; G. Simultaneous Determination of Levodopa and Carbidopa from Fava Bean, Green Peas, and Green Beans by High Performance Liquid Gas Chromatography. *J. Clin. Diagn. Res.* **2013**, *7* (6), 1004−1007.
(48) Rabey, J. M.; Vered, Y.; Shabtai, H.; Graff, E.; Korczyn, A. D. Improvement of Parkinsonian Features Correlates with High Plasma Levodopa Values after Broad Bean (Vicia faba) Consumption. *J. Neurol., Neurosurg. Psychiatry* **1992**, *55* (8), 725−727.
(49) Schmelzeisen-Redeker, G.; Schoemaker, M.; Kirchsteiger, H.; Freckmann, G.; Heinemann, L.; Del Re, L. Time Delay of CGM Sensors: Relevance, Causes, and Countermeasures. *J. Diabetes Sci. Technol.* **2015**, *9* (5), 1006−1015.
(50) Martin, C. T.; Criego, A. B.; Carlson, A. L.; Bergenstal, R. M. Advanced Technology in the Management of Diabetes: Which Comes First—Continuous Glucose Monitor or Insulin Pump? *Curr. Diab. Rep.* **2019**, *19*, 50.

https://doi.org/10.1021/acssensors.6c02083
ACS Sens. XXXX, XXX, XXX−XXX